ISOPHOT - PHOTOMETRIC CALIBRATION OF POINT SOURCES

**B. Schulz[1,2], S. Huth[2,3], U. Kinkel[2,3*], D. Lemke[3],
J. Acosta[1,2,3,4], M. Braun[2,3,7], H. Castañeda[2,3,4], L. Cornwall[2,5], C. Gabriel[1,2],
I. Heinrichsen[2,6,8], U. Herbstmeier[3], U. Klaas[2,3], R. Laureijs[1,2], T. Müller[1,2,3]**

[1] ISO Data Centre, ESA Astrophysics Division, Villafranca del Castillo, Spain
[2] ISO Science Operations Centre, ESA Astrophysics Division, Villafranca del Castillo, Spain
[3] Max-Planck-Institut für Astronomie, Heidelberg, Germany
[4] Instituto de Astrofisica de Canarias, Tenerife, Spain
[5] Rutherford Appleton Laboratory, Chilton, UK
[6] Max-Planck-Institut für Kernphysik, Heidelberg, Germany
[7] Astrophysikalisches Institut Potsdam, Germany
[8] Infrared Processing and Analysis Center, JPL, Pasadena, USA

ABSTRACT

We discuss the photometric calibration of ISOPHOT for point sources in the wavelength range from 3.2 to 240 μm for the aperture photometer (PHT-P) and the FIR camera section (PHT-C). To correct for temporal drifts of detector responsivities, all observations included reference measurements against stable internal sources. These have been absolutely calibrated in-orbit against well known celestial standards. In this process corrections were derived for instrumental effects like nonlinearities, signal-transients, time variable dark current or misalignments. For staring- or raster-observations of point sources in standard configurations, the scatter of the individual data points around the derived calibration relations is a measure of the consistency and typical accuracy of the calibration.

Key words: ISO; infrared astronomy; calibration; data-reduction; ISOPHOT.

1. INTRODUCTION

The imaging photopolarimeter ISOPHOT (Lemke et al. 1996) onboard ESA's Infrared Space Observatory ISO (Kessler et al. 1996) features photoconductors as infrared detectors, made from doped Silicon and Germanium. Since the detectors exhibit a varying response to IR-radiation, mostly due to cosmic particle hits but also due to the IR flux history, an internal fine calibration source (FCS), radiating similar to a grey-body, is used as stable reference. Electrical heating of the FCS with powers of 0.001 to 50 mW, generates a range of highly reproducible fluxes over more than 5 orders of magnitude.

*deceased 1997

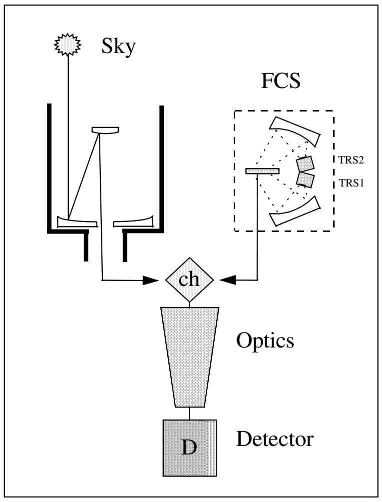

Figure 1. Calibration scheme. The detector receives IR-radiation either from the sky or from the internal calibration source (FCS), switching beams with the chopper-mirror (ch).

2. CALIBRATION SCHEME

By observing celestial standards followed by measurements of the FCS at similar brightness, we calibrated the FCS absolutely over the full accessible flux-range of the 25 filter bands as outlined in Figure 1. In turn the routine astronomical observing sequences were calibrated by including at least one FCS-measurement into each sequence, that allowed to reestablish the detector responsivity $R = I_{phot}/P_{src}$ for the time of the observation, i.e. the ratio between measured photocurrent I_{phot} and corresponding infrared inband power on the detector P_{src}. We calculate the inband power for standard point sources as $P_{src} = A_{tel}\, f_{PSF_{f,a}}\, T_{refl.} \int [T_f(\lambda)\, R_p(\lambda)\, F(\lambda)]\, d\lambda$, where A_{tel} is the area of the telescope primary, $f_{PSF_{f,a}}$ the fraction of the light of a point source falling through the selected filter f into the detector aperture a, $T_{refl.}$ the reflection losses of all mirrors in the optical path, $T_f(\lambda)$ the spectral transmittance of the filters and field lenses, $R_p(\lambda)$ the relative spectral response function of the detector pixel p, normalised to the peak response, and $F(\lambda)$ the spectral energy distribution of the point source. Note that including $R_p(\lambda)$ makes the detector responsivity R filter independent for the same detector pixel. We ignore the small systematic error arising from the simplified colour independent PSF correction factor.

To convert inband powers to flux densities F_ν, for the normal case of objects with initially unknown SED, the relation $P_{src} = F_\nu\, C1_f\, f_{PSF_{f,a}}$ is used, where the conversion factors $C1$ are calculated for an assumed reference spectrum of $\nu F_\nu = const.$ The result still needs to be corrected for the actual colour of the object, once this is known.

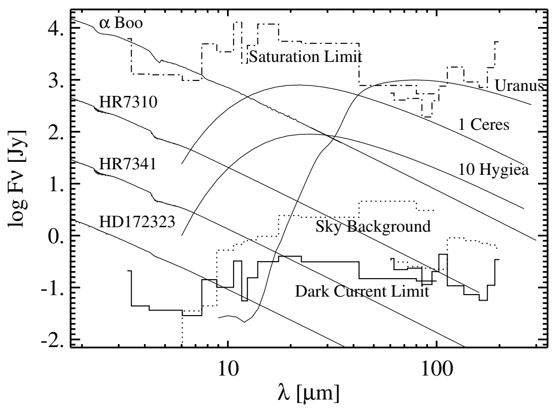

Figure 2. The coverage of the flux domain accessible to ISOPHOT by celestial standards. SEDs of examples of the three source types are plotted as solid lines (c.f. Tables 1 and 2 for relative brightnesses). Upper and lower flux limits due to saturation, sky background and dark current are indicated (there are separate lines for PHT-P and PHT-C which overlap).

3. CELESTIAL STANDARDS

The photometric calibration of ISOPHOT is based entirely on point sources, which constitute the best known infrared fluxes in the sky. The sources are observed either with PHT-P in a standard circular aperture that is defined per filter (23 arcsec for 3.3-7.7 μm, 52 arcsec for 10-16 μm, 79 arcsec for 20-25 μm and 180 arcsec for 60-100 μm), or with PHT-C in each pixel (43.5 and 89.4 arcsec pixelsize). As the detailed radiation spectrum of the FCS was unknown and linearity of the detectors could not a priori be postulated, the empirical FCS calibration required the availability of calibration standards covering the full observable flux range between 3 and 240 μm. The upper flux limit is determined by the dynamic range of the cold readout electronics (CRE) and the detector responsivity. The lowest signals are determined by the celestial background (Zodiacal Light, Galactic Cirrus) and at short wavelengths by the dark current. Figure 2 shows these limits projected into the flux domain. The flux/wavelength range between is well covered by stars, planets and asteroids.

Table 1. The list of stars used for ISOPHOT calibration. The brightnesses are given in the P_11.5 and C_60 filters, depending on the usage in the range 3-30 μm or 45-240 μm respectively. The magnitudes were calculated with respect to the photometric system defined by the ISOPHOT filters with the Kurucz model of Vega as zero point.

Stellar Celestial Standards

Name	2nd name	type	mag (P_11.5)	mag. (C_60)
HD172323	-	F9V	6.55	
HD184400	-	F5	7.53	
HR337	β And	M0IIIv	-2.05	-2.17
HR617	α Ari	K2III	-0.76	-0.83
HR1457	α Tau	K5III		-3.12
HR1654	ϵ Lep	K5IIIv		-0.43
HR3748	α Hya	K3II-III	-1.31	-1.39
HR5340	α Boo	K1III	-3.15	-3.22
HR5886	-	A2IV	5.09	
HR5986	-	F8IV-V	2.71	
HR6514	-	A4V	6.14	
HR6688	-	K2III		0.92
HR6705	γ Dra	K5III	-1.46	-1.56
HR6847	-	G2V	4.76	
HR7001	α Lyr	A0V	0.00	
HR7310	-	G9III	0.67	0.67
HR7341	-	K1III	3.64	
HR7451	-	F7V	4.51	
HR7469	-	F4V	3.51	
HR7633	-	K5II-III	1.14	1.11
HR7742	-	K5III	2.18	
HR7980	ω Cap	M0III		-0.08
HR8684	-	G8III	1.27	
HR8775	β Peg	M2.5II-I	-2.44	-2.54

The ISO Ground Based Preparatory Program (GBPP) (Jourdain de Muizon & Habing 1992, Van der Bliek et al. 1992, Hammersley et al. 1998) provided stellar spectra up to wavelenths of 50 μm. FIR extrapolations were provided too. In the range between 2 and 160 μm the SEDs have attributed uncertainties between 3 to 5 per cent. Above 160 μm all quoted errors are 5 per cent. Another calibration programme by Cohen et al. (1996) provided SEDs in the range of 1.2 to 35 μm. To extrapolate to 240 μm, Engelke functions (Engelke 1992) were used. The typical absolute accuracy of the templates is about 3 per cent, for the FIR extensions longward of 25 μm 6 per cent are assigned. Both programs used Kurucz model atmospheres of Sirius and Vega as common zeropoint for their broadband photometry. Table 1 lists the stars actually used for ISOPHOT calibration.

Uranus and Neptune are commonly used as submillimeter and FIR standards. They provided the highest calibrated flux levels between 45 and 200 μm. Model SEDs of both planets were kindly provided for all dates of ISOPHOT observations by Abbas et al. (1997). The models take into account tempera-

Table 2. The list of planets and asteroids used for the calibration in the 45-240 μm range. We give the range of magnitudes occurring during visibility intervals of the given object over the ISO mission.

Solar System Standards

source name		mag (C_60)
Uranus		-7.21...-7.28
Neptune		-6.01...-6.07
1	Ceres	-5.85...-6.46
2	Pallas	-4.23...-5.67
3	Juno	-3.81...-4.36
4	Vesta	-5.34...-6.03
10	Hygiea	-3.52...-3.97
54	Alexandra	-3.13...-3.42
65	Cybele	-2.69...-3.24
106	Dione	-1.32...-1.35
313	Chaldaea	-2.10...-2.15
532	Herculina	-2.91...-3.99

ture profiles, CH_4 mixing ratios and absorption by H_2 and He. These were obtained directly from Voyager IRIS and RSS instrument data, supplemented by model profiles from Abbas et al. (1997) or taken from Lindal (1992) for Neptune. Comparison with other models for Uranus (Griffin & Orton 1993) and for Neptune (Lellouch 1997), showed consistency within 10-20 per cent between 240 and 30 μm. Larger discrepancies appear below 30 μm in a regime, where H_2 and He absorption becomes a major factor.

Some asteroids are well enough understood by thermophysical modelling in order to be used as FIR standards. They can fill the gap at intermediate flux levels, that appears at wavelengths between 45 and 200 μm between planets and stars(see Figure 2). Some specific complications arise, since they are moving objects w.r.t. the sky background and show periodic variations of their intensity due to rotation and varying distance to the Earth and Sun. For the actual photometric calibration a Thermophysical Model (TPM) (Müller & Lagerros 1998) is used. The TPM assumes a rotating ellipsoid, thus accounting for lightcurve variations, and parametrises heat conduction, surface roughness and scattering in the regolith. The final accuracy of the standards is ±10 per cent in the wavelength range from 24 to 500 μm, except for 106 Dione and 65 Cybele, where discrepancies between model and observations of 20-30 per cent were found. Table 2 lists the solar system objects, that were actually used for ISOPHOT calibration.

4. DATA REDUCTION

Each calibration observation consisted of 4 different measurement types: on source, off source, heated FCS and cold FCS (FCS straylight). The data was reduced automatically by a dedicated software package as described in Huth & Schulz (1998), using PIA as a basis (Gabriel et al. 1997). Reducing the measured integration ramps homogeneously to signals in units of V/s, i.e. S_{src}, S_{bck}, S_{fcs}, S_{str} respectively, it applies the standard corrections for ramp nonlinearities, signal dependence on readout timing and glitches. Moreover it includes an automatic transient correction algorithm and a quality flag system. For each FCS measurement the inband power corresponding to the FCS heating power h is calculated according to $P_{fcs}(h) = \frac{(S_{fcs}(h)-S_{str})\,P_{src}}{S_{src}-S_{bck}}$. This assumes linearity of the detector over the flux range spanned by the measurements of celestial standard and FCS. The results form the basis for the derivation of several calibration tables and further investigation of calibration issues.

5. PHOTOMETRIC CALIBRATION

The fundamental calibration tables are called FCS power curves and contain the relation between FCS heating power h and FCS inband power P_{fcs} (see Figure 3). They are determined directly from the data by polynomial fits for each of the 25 filter bands. For the aperture photometer the table $P_{fcs}(h)$ is expressed in units of [W/mm^2] since the FCS appears as an extended source. The values are multiplied by the area A of the field aperture, to derive the FCS inband power on the detector. Since the illumination of the apertures is not perfectly homogeneous, systematic deviations appear for different apertures. Therefore the results presented here do only apply for the standard apertures. For the array detectors the FCS power curves are already in units of [W], however since they also are illuminated inhomogeneously by the FCS, the average power curve needs to be corrected for each individual pixel by the illumination matrix $\Gamma_{p,f}$. This matrix depends also on filter. The responsivity R as defined above is independent of filter. Systematic differences found between different filters of the same detector pixel, independent of the celestial standard, are corrected by the filter to filter correction table $\chi_{p,f}$. These corrections are different for different pixels of the same array detector, due to spatial inhomogeneities across the broadband filters.

Using the derived tables of calibration parameters, an ISOPHOT observation of a point source is calibrated as follows. First, the responsivity of each detector pixel is determined from the FCS measurement. For P-detectors according to:

$$R_p = \frac{(S_{fcs_{p,f}} - S_{str_{p,f}})\,C_{int}}{P_{FCS_f}(h)\,A\,\chi_{p,f}} \tag{1}$$

and for C-detectors according to:

$$R_p = \frac{(S_{fcs_{p,f}} - S_{str_{p,f}})\,C_{int}}{P_{FCS_f}(h)\,\Gamma_{p,f}\,\chi_{p,f}} \tag{2}$$

We use 90 fFarad as value of the integration capacity of the CRE C_{int}, except for C200, where it is 140 fFarad. The FCS straylight signal $S_{str_{p,f}}$ was always measured in the calibration observing sequences, but was not measured in each astronomical observing sequence. In general it is close to the dark current signal.

Next the sky signals $S_{p,f}$ are converted into an inband power by

$$P_f = \frac{S_{p,f}\,C_{int}}{R_p\,\chi_{p,f}}. \tag{3}$$

Note that the source measurement does not need to be in the same filter band as the FCS measurement, however, if so, $\chi_{p,f}$ cancels out and the systematic uncertainty associated with this table is removed from the error budget. The conversion to flux density is performed as explained above.

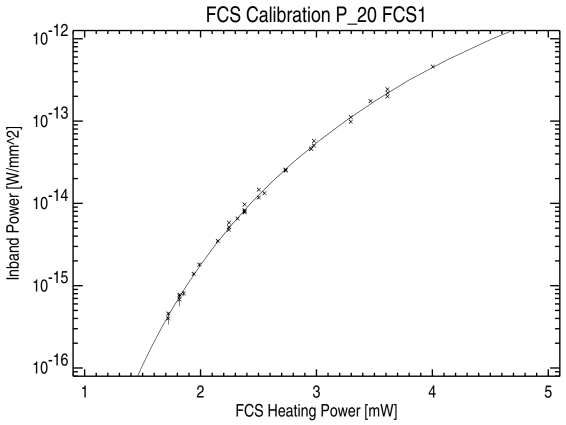

Figure 3. Example of an FCS power curve plotted with the measured data.

6. ACCURACIES

We assess the accuracy of the instrument in terms of reproducibility and consistency of the photometric results.

The photometric system stability depends mainly on the stability of the FCS and the reproducibility of the detector transient behavior. In a long term monitoring program measurements on NGC6543 were repeated every 5 weeks and on some fainter stars every 2 weeks. For the bright planetary nebula we found a standard deviation among the results between 2 and 7 per cent, the fainter sources show larger scatters of 7 to 12 per cent due to longer transients, glitches and structured background.

The photometric consistency was determined by comparing the FCS power curves and the datapoints they were derived from. Figure 3 shows an example of a power curve, in this case for the filter P_20 with the measured data points. Each FCS heating power corresponds to an FCS inband power that is individually calibrated by a celestial standard. Since the curve is known to be smooth and the calibration observations passed the same reduction steps as every science observation, the scatter around the fitted polynomial is representative for the photometric uncertainty of staring or raster observations. Uncertainties of the celestial calibration standards (section 3) and within the signal determination, increase the scatter. Only a photometric bias among the standards would not be seen. Table 3 shows the scatter that was calculated as the standard deviation of all values $P_{Cal-G}(h)/P_{meas.}(h) - 1$ of one filter, where P_{Cal-G} is the inband power from the FCS power curve and $P_{meas.}$ is the corresponding measured one. For the array detectors C100 and C200 the scatter calculation included all pixels. The range of inband powers of each detector was divided into an upper and a lower part to account for the gradual increase of the scatter towards smaller fluxes. The splits are at 100, 200, 20, 5 and 10 $\cdot 10^{-15}$ W for P1, P2, P3, C100 and C200 respectively. Again the scatter is larger for smaller fluxes. For multi filter measurements the uncertainty of the filter to filter calibration matrices χ of 2 to 9 per cent has to be included into the overall error budget. The photometric accuracies we find for the FCS calibration are consistent with results from comparisons of dedicated validation observations and data from the literature (see Lemke et al. 1998).

Table 3. Comparison of derived FCS power curves with measured calibration data. n is the number of measurements used, max. is the maximum deviation found in per cent, σ_{lo} and σ_{hi} are the standard deviations in per cent for the low and high part of the fluxes.

detector	n	max per cent	σ_{lo} per cent	σ_{hi} per cent
P1	148	47	14	10
P2	54	72	16	5
P3	93	77	26	21
C100	1788	146	18	14
C200	878	54	14	8

ACKNOWLEDGMENTS

We like to thank M. Abbas, M. Cohen, P. Hammersley, D. Osip and C. Telesco for their support, in particular the many SEDs of calibration standards. Furtheron we thank all our colleagues at VILSPA and MPIA for their efforts to make ISO a success.

REFERENCES

Abbas, M., Osip, D., Romani, P.1997, priv. comm.

Van Der Bliek, N.S., et al. 1992, ESO Mess., 70, 28

Cohen, M. et al. 1996, AJ, 112, 2274

Engelke, C. W. 1992, AJ, 104, 1248

Gabriel, C., at al. 1997, Proc. of the ADASS VI conference, eds. Hunt, G. & Payne, H.E., p. 108

Griffin, M. J. & Orton, G. S. 1993, Icarus, 105, 537

Hammersley, P. L., et al. 1998, A&AS, 128, 207

Huth, S. & Schulz, B., 1998, ASP Conf. Ser. 145: ADASS VII, 7, 212

Jourdain de Muizon, M. J.-D., Habing, H. 1992, Les Houches Series: Infrared Astronomy with ISO, Th. Encrenaz, M.F. Kessler eds., pp 129-138

Kessler, M.F. et al. 1996, A&A, 315, L27

Lellouch, E., 1997, priv. comm.

Lemke, D., Klaas, U., et al. 1996, A&A, 315, L64

Lemke, et al. 1998, this volume

Lindal, G. 1992, AJ, 103, 967

Müller, T. & Lagerros, J. 1998, A&A, 338, 340